Dynamic Response of Cross Steel Reinforced Concrete Filled Steel Tubular Columns under Impact under Fire

Zhi Li[1,2], Teng-Fang Dong[1,2], Feng Fu[2,3], and Kai Qian[1,2]*

1. Guangxi Key Laboratory of New Energy and Building Energy Saving, Guilin University of Technology, Guilin 541004, Guangxi, China;

2. College of Civil Engineering and Architecture, Guilin University of Technology, Guilin 541004, Guangxi, China

3 Department of Engineering School of Science and Technology City, University of London, Northampton Square, London EC1V 0HB, United Kingdom

Abstract:

To explore the impact response of cross steel-reinforced concrete-filled steel tubular (CSRCFST) columns under fire, a finite element model using ABAQUS software was generated. After validation against test results, parametric studies were carried out to investigate the effects of impact load as well as time of fire exposure on the impact resistance of CSRCFST columns. The numerical results show that the impact behavior of post-fire CSRCFST columns can be divided into three stages: peak stage, plateau stage, and softening stage. For CSRCFST columns, the peak and plateau stages are important, which absorbed 32.4 % and 67.6 % of the impact kinetic energy, respectively. After two hours of fire exposure, the stiffness and peak impact load of the column decreased by 93.7 % and 71.7 %, respectively. However, the peak mid-span deflection and residual deflection increased by 6.5 % and 20.1 %, respectively. When the drop weight tripled, the maximum deflection and residual deformation of the midspan increased by 2.8 and 3.2 times, respectively. However, the peak impact load increases only by 14.5 %. When the impact energy is the similar, the maximum midspan deflection of the specimen is almost identical, whereas a larger impact momentum reduces the peak

impact force but increases the impact force at the plateau stage. By increasing fire duration, the behaviors of the column deteriorate seriously, with 85% reductions in peak impact force and 39% increase in maximum midspan deflection. In addition, the effects of impact velocity are also significant regarding each stage.

Keywords: CSRCFST; Post-fire; Impact behavior; Numerical simulation; Column

* Corresponding author. E-mail address: qiankai@glut.edu.cn

1 Introduction

Accidental loads such as explosion, fire, and vehicular impact may cause partial destruction of the building structure and lead to a disproportionate collapse of the whole structure [1, 2], bringing serious consequences. Therefore, studies on the progressive collapse behavior of structures are needed [3-8]. The engineering practice shows that the building structure is often accompanied by subsequent impact load when fire occurs. For example, in 2001, the Twin Towers of the World Trade Center in the United States collapsed progressively after being hit by a passenger plane hijacked by terrorists, causing serious casualties. Subsequent studies show that the large area fire caused by aircraft impact is the main reason that resulted in the collapse of that building [9, 10]. Therefore, it is essential to study the progressive collapse behavior of building structures under the coupling action of fire and impact.

Wang et al. [11] proposed a new type of composite structure, namely Cross Steel Reinforced Concrete Filled Steel Tubular (CSRCFST) structure based on its structure with good compressive, flexural, and shear bearing capacity and deformation capacity [12, 13] but relatively poor fire resistance [11], as shown in Fig. 1. At present, many scholars have carried out relevant studies on the fire resistance and impact resistance of Concrete Filled Steel Tubular (CFST) and CSRCFST structures, respectively. Wang et al. [14] conducted an experimental study on CFST components under the horizontal impact, and the study showed that axial load could improve the impact performance of components to a certain extent. Han et al. [15] studied the impact resistance of high-strength CFST members by experimental research and numerical simulation and proposed a simplified model for calculating dynamic flexural bearing capacity of CFST members based on the results. Rifaie et al. [16] investigated the structural behavior of CFST columns connected by long bolts and end plates under horizontal impact load. The results showed that when thicker end-plate was used the impact resistance of CFST columns would be weakened, the fracture of bolts would be accelerated, and the energy consumption would be reduced. Zhu et al. [17] studied the impact behavior of CSRCFST columns under different impact velocity, height, axial load, steel tube thickness, and boundary conditions. It was found that the external square steel tube can effectively protect the internal concrete, and the steel tube was the main energy dissipation source of the structure. Li et al. [18] conducted a study on the surface thermal emissivity and thermal response of CFST columns in high temperature environment, and it showed that the smaller the surface thermal emissivity of the columns, the better the fire resistance of the structure. Li et al. [19] studied the fire resistance limit of CFST columns under different variable parameters such as steel yield strength, concrete compressive strength, and the thickness of the fire protection layer of lightweight aggregate concrete. The results showed that lightweight aggregate concrete can effectively improve the fire resistance of columns. Wang et al. [20] carried out experimental and numerical studies to figure out the effects of initial geometrical defects, residual stress, multi-factor coupling, and other variable parameters on the fire response characteristics of CFST columns. The results showed that the core concrete can effectively reduce the specific heat and maximum temperature of the external steel tube, and the initial geometric defects will produce load eccentricity on CFST columns, reducing its fire resistance. Ji et al. [21] studied the lateral impact performance of post-fire CSRCFST components. The designed variables are fire duration, drop hammer to columns mass ratio and axial compression ratio. The results showed that the maximum mid-span deflection of the column increased by 41 % and the impact force plateau decreased by 27 % after exposure to fire for 3 hours. The energy absorbed by the plastic deformation of the steel tube accounted for about 72 % of the whole column.

To sum up, there are relatively few studies on impact behavior of CSRCFST structures at present. Most of the available studies are only considering single action, fire or impact load, and there are few studies on the coupling action of fire and impact.

Therefore, based on the CSRCFST structure proposed by Wang et al. [11] and the impact test at room temperature conducted by Zhu et al. [17], this paper deeply studied the impact dynamic behavior of CSRCFST columns under fire by using finite element (FE) analysis method. The specific research technical route of this paper is as follows. Firstly, the impact test at room temperature is simulated and verified. On the basis of verifying the validity of the model, the impact dynamic performance of the column under fire is further studied. Finally, the variable parameters such as impact mass and impact momentum are expanded and analyzed. It provides necessary helps for design engineers to design CSRCFST columns considering the coupling effects of fire and impact.

2 FE Modeling and verification

2.1 Introduction to the program of the validation tests

The impact tests conducted by Zhu et al. [17] in room temperature is shown in Fig. 2. Ultraheavy drop hammer was adopted, with a total mass of 1158.7 kg, a hammer head size of 300×300×200 mm^3, and an impact contact surface between the bottom of the hammer head and the column of 300×300 mm^2. The fixed support consisted of a bottom and a top head and was bolted to a rigid platform. When the axial force was applied, it was first applied on the disc springs through a 200-Ton hydraulic jack fixed on the reaction frame, and then the axial force was transmitted to the column through the disc spring. At the same time, the right end of the columns was reserved for 25 mm extended support. The total column length was 1800 mm and the cross-section was 300×300 mm^2. Moreover, the thickness of the outer steel tube was 8 mm. 225 mm and 350 mm lengths on the left and right sides of the column were reserved for fixed supports, so the effective length of the column was 1200 mm. The dimensions of cross-shaped steel profiles inside the column was 200×100×6×9 mm. To make the force uniform and prevent the column from local deformation under axial load, a steel plate with width of 300 mm, and a thickness of 20 mm was added at both ends of the column. The column reinforcement details and dimensions are shown in Fig. 3.

In the fire test conducted by Zhu et al. [22], the electric heating furnace device was used to heat up the three surfaces of the CSRCFST columns, and the heating process was carried out according to the ISO 834 standard heating curve [23].

2.2 FE Model setup

The impact tests at room temperature were validated by the three typical columns in reference [17], and their variables were shown in Table 1. Where H is the impact height, and V is the instantaneous impact velocity of the drop hammer. The axial compression ratio n is defined as $n = N_0 / N_u$, where N_0 is the axial force of column and N_u is the nominal ultimate axial capacity of CFST square column. The design strength of concrete was C40, and the average yield strength (f_y), ultimate strength (f_u), elastic modulus (E_s), and elongation ratio (δ) of steel with different thickness are shown in Table 2.

The general-purpose software ABAQUS was used to model the impact tests column under room temperature. The hammer head was simulated using a discrete rigid body and imposed isotropic mass by defining reference points. Steel tube and steel profile adopt S4R elements, and concrete and support was simulated using C3D8R elements.

For steel, according to the five-stage elastoplastic constitutive model of Han **Error! Reference source not found.**, the stress-strain curve is shown in Eq. (1a) ~ Eq. (1e)[24]:

$$\sigma = E_s \cdot \varepsilon \qquad \varepsilon \le \varepsilon_1 \tag{1a}$$

$$\sigma = -A \cdot \varepsilon^2 + B \cdot \varepsilon + C \qquad \varepsilon_1 \le \varepsilon \le \varepsilon_2 \tag{1b}$$

$$\sigma = f_{sy} \qquad \varepsilon_2 \le \varepsilon \le \varepsilon_3 \tag{1c}$$

$$\sigma = f_{sy} \cdot \left[1 + 0.6 \cdot \frac{\varepsilon - \varepsilon_3}{\varepsilon_4 - \varepsilon_3} \right] \qquad \varepsilon_3 \le \varepsilon \le \varepsilon_4 \tag{1d}$$

$$\sigma = 1.6 \cdot f_{sy} \qquad \varepsilon > \varepsilon_4 \tag{1e}$$

where, E_s=200,000MPa, $\varepsilon_1 = 0.8 \cdot f_{sy} / E_s$, $\varepsilon_2 = 1.5 \cdot \varepsilon_1$, $\varepsilon_3 = 10 \cdot \varepsilon_2$, $\varepsilon_4 = 100 \cdot \varepsilon_2$, f_{sy} is the yielding strength of the steel. And the stress-strain curve is shown in fig. 5, $f_{sp} = 0.8 f_{sy}$, $f_{su} = 1.6 f_{sy}$.

According to Cowper-Symonds [25] constitutive model, the strain rate effect under high-speed motion was considered, as shown in Eq. (2):

$$f_y^d / f_y = 1 + (\dot{\varepsilon} / D)^{1/p} \tag{2}$$

where f_y^d is the yield strength of steels under strain rate $\dot{\varepsilon}$ while f_y is the yield strength of steel rebar. Meanwhile, it was assumed that the strain rate effect does not change along with the strain hardening. The values of D and p are set as 6844 s^{-1} and 3.91, respectively.

For concrete, CDP model [26] and the constitutive model of steel tube confined concrete proposed by Han et al. [24] were adopted, the stress-strain curve is shown in Fig. 6, where the confinement factor ξ is defined as:

$$\xi = \frac{A_s \cdot f_{sy}}{A_c \cdot f_{ck}} \tag{3}$$

where A_s is the cross-section area of steel tube, A_c is the cross-section area of concrete, f_{sy} is the yield stress of steel tube and f_{ck} is the compression strength of concrete. The value of f_{ck} is determined using 67 % of the compression strength of cubic blocks.

And the strain rate effect [25] is considered, the relationship between the dynamic compressive strength of concrete and strain rate is shown in Eq. (4):

$$f_d / f_c^{'} = (\dot{\varepsilon}_d / \dot{\varepsilon}_s)^{1.026\alpha} (\dot{\varepsilon}_d \leq 30\,\mathrm{s}^{-1})$$

(4)

where f_d (N/mm^2) is the dynamic compressive strength of concrete; $f_c^{'} = f_{ck} + 8(\mathrm{N/mm^2})$, f_{ck} is the characteristic static compressive strength of concrete; $\dot{\varepsilon}$ is the strain rate(s^{-1}); $\dot{\varepsilon}_s = -30 \times 10^{-6}\,\mathrm{s}^{-1}$ is the static strain rate; $\alpha = 1/(5 + 9 f_c^{'} / f_{co})$; $f_{co} = 10(\mathrm{N/mm^2})$.

The relationship between the dynamic tensile strength of concrete and strain rate [25] is shown in Eq. (5):

$$f_{td} / f_t = \begin{cases} (\dot{\varepsilon}_d / \dot{\varepsilon}_s)^{\delta} & \dot{\varepsilon}_d \leq 1\mathrm{s}^{-1} \\ \beta(\dot{\varepsilon}_d / \dot{\varepsilon}_s)^{1/3} & \dot{\varepsilon}_d > 1\mathrm{s}^{-1} \end{cases} \tag{5}$$

where f_{td} is the dynamic tensile strength of concrete; f_t is the static tensile strength of concrete; $\dot{\varepsilon}_d$ is the strain rate (s^{-1}) in the range of 10^{-6} to 160 s^{-1}; $\dot{\varepsilon}_s = 1 \times 10^{-6}\,\mathrm{s}^{-1}$ is the static strain rate; $\log \beta = 6\delta - 2$; $\delta = 1/(1 + 8 f_c^{'} / f_{co})$; $f_{co} = 10(\mathrm{N/mm^2})$.

In the model, the normal direction of all contact interfaces was hard to contact, and the tangential direction was coulomb friction. The friction coefficient between concrete and steel was 0.6, and that between drop hammer and steel was 0. The end-plates were connected to the cross section by “Tie” interaction. Impact velocity was applied through predefined fields. At the same time, to facilitate subsequent data processing, the drop hammer was placed at a certain distance above the columns according to different impact velocities, so that all the columns had an impact at 0.005 s. The schematic diagram of the model is shown in Fig. 7.

The validation of heat transferring analysis using the results of column S3H-0.3 in reference [22]. Accordance to GB5249-2017 [28] and Lie et al. [29], thermal parameters, such as thermal conductivity, specific heat and thermal expansion coefficient, and constitutive relations of steel and concrete were defined during modeling. The strain rate effect of steel and concrete under high temperature is not well studied at present, and the applications of its achievements in FE simulation are still lacking. As the degree of material degradation caused by high temperatures is more evident than that caused by strain rate, the strain rate effect parameters at room temperature are still used for steel and concrete exposed to fire. The ISO 834 fire standard heating curve [23] was adopted to uniformly heat up the three sides of the column in fire for 120 mins. The interaction of exposed surfaces includes thermal convection and radiation, and the coefficient of thermal convection and radiation are 25 W/(m^2·℃) and 0.5, respectively. “Tie” was used to constrain components. Concrete adopted DC3D8 heat transfer entity, while steel tube and section steel were DS4 elements. The schematic diagram of the model is shown in Fig. 8.

2.3 Model validation

Fig. 9 shows the time history curves of impact force and mid-span deflection obtained from the impact column test from [17] and simulation. As shown in Fig. 9, the simulated time history curves of impact force matched well with the test curves. The average ratio of peak impact force (FEM Fmax/TEST Fmax) was 0.9869, and the Cov. was 0.1122. The average ratio of peak mid-span deflection (FEM D_{max}/TEST D_{max}) was 0.9804, and the Cov. was 0.04. Fig. 10 shows the heating time history curves at different measuring points obtained from the fire column test and simulation and the ISO 834 standard heating curve. It can be seen from the figure that the, peak temperature of heating and failure mode of the two were quite consistent.

Therefore, in general, the FE model in this paper can well predict the time-history curve of impact force, mid-span deflection, and internal heating curve of CSRCFST column under impact load. It can be used for coupled thermo-mechanical analysis of impact and fire action.

3 Impact behavior of CSRCFST columns under fire

3.1 Coupled thermo-mechanical model

To further explore the impact resistance of CSRCFST columns at high temperature of fire, the thermal-mechanical coupling method was used to establish the impact model under fire. Firstly, the normal temperature impact model S8HFF2 was used as the basic model, and the axial compression ratio *n* was kept at 0.2. Then the ODB file of the FE model for three-sided heat transfer analysis under uniform fire for 120 mins was imported into the ' predefined field ' of the basic model.

The constitutive relation of materials under fire was referred to the literature [27] and [30]. The interaction between steel profile and concrete was constrained by embedding while the contact model between other columns was changed to general contact. Concrete and end-plates were modelled by C3D8R elements while the steel tubes and steel profiles were modelled by S4R elements.

3.2 Impact process analysis

The impact force (F), mid-span displacement (Δ_1), mid-span velocity (V_1), drop weight displacement (Δ_2), and drop weight velocity (V_2) during the impact testing of the column under fire were converted into normalized time-history curves, as shown in Fig. 11. The ratio of column mid-span displacement (Δ_1), velocity (V_1) to the displacement (Δ_2) and velocity (V_2) of the drop weight was used to obtain the time-history diagram of the ratio of displacement and velocity between the column and the drop weight, as shown in Fig. 12.

It can be seen from the figures that the impact history of the column under the fire was divided into four stages: the peak stage (AB), the plateau stage (BC), the softening stage (CD), and the post-impact stage (DE).

The peak stage is the time period from the falling weight starting to hit the column until the impact force reaches peaks. At this stage, the high-speed drop hammer vertically impacted the mid span of the column, and the column impact force rapidly reached the peak value within 0.0003 s. The mid span began to develop deflection, and the velocity changed and reached the peak value. Subsequently, the drop hammer and the column begin to move downward together. But the drop hammer velocity was greater than the mid-span velocity, and the energy was gradually transferred from the drop hammer to the column. At the end of the peak stage, the drop hammer velocity decreased by 17.8 %, and 32.4 % of the kinetic energy was converted into the kinetic energy and strain energy of the column.

The plateau stage is the period from the peak impact force to the maximum deflection of the column. At this stage, the drop hammer was still in contact with the column, and the falling velocity continued to decrease, but it was still greater than the mid-span velocity. 67.6 % of the kinetic energy continued to be converted into the kinetic energy and strain energy of the column. At the same time, the impact force dropped sharply and maintains a relatively stable value. The mid-span deflection continued to increase until reaching the maximum, and the velocity began to drop to 0 m/s. The velocity of the drop weight decreased to 0 m/s, and all the remaining kinetic energy is converted into the kinetic energy and strain energy of the column.

The softening stage is the period from the maximum deflection of the column until the impact force drops to 0 kN. At this stage, the drop hammer and the column began to rebound upward. All the kinetic energy of the drop hammer was consumed and transformed. The maximum deflection in the column span was reached. The strain energy was transformed into its own kinetic energy and the kinetic energy of the drop hammer, and the mid-span velocity was greater than the drop hammer velocity. At the same time, the column impact force decreased from a relatively stable value to 0 kN. The mid-span deflection rebound decreased, and the velocity increased inversely and then decreased to 0 m/s.

The post-impact stage refers to the period after the impact force drops to 0 kN. At this stage, there was no interaction between the drop hammer and the column, but the column still has a small amplitude of natural vibration, and there was residual deflection in the mid-span position.

3.3 Comparison between room temperature and fire

Fig. 13 shows the comparison of the impact force versus mid-span deflection time history curve of the column under room temperature and fire. It can be seen from the figure that there was a great difference between the impact dynamic response of the column under these two conditions. The impact stiffness of the column under room temperature and fire was 119.2 kN/mm and 7.5 kN/mm, respectively. The impact stiffness of column under fire decreased by 93.7 %. The peak impact force under room temperature and fire was 23.9 kN and 6.8 kN, respectively. The peak impact force under fire decreased by 71.71 %. The maximum mid-span deflection of the column under fire and room temperature was 23.0 mm and 21.6 mm, respectively. The maximum mid-span deflection of the columns under fire increased by 6.50 %. The residual deflections of columns under fire and room temperature were 18.5 mm and 15.4 mm, respectively. Thus, the residual deflections of columns under fire increased by 20.1 %. The comparison shows that under high temperature of fire, the column material performance deteriorates, the overall strength decreases, the stiffness weakens, and the mid-span deflection and residual deflection generated by impact are larger.

3.4 Axial force and support reaction force

Fig. 14 shows the time-history curves of axial force and support reaction force (excluded column gravity) in the process of column impact under fire. It can be seen from the figure that at the peak stage, axial force and support reaction force increased rapidly. When the axial force reached the peak value of 895.6 kN, the unloading began, and the support reaction increased to 367.1 kN. This was because at the moment of impact, the shock wave spread from the mid-span area along the column to both sides of the support, squeezing the spring and increasing the axial force. Then, due to the continuous deformation of the column, the horizontal distance of the beam end decreased, so that the spring was extruded to elongate, and the axial force began to unload and increased in reverse. At the same time, the column was subjected to the impact force of the falling hammer, resulting in upward reaction force. In the plateau stage, the axial force continued to increase to the peak value of 746.9 kN and then vibrated. The support reaction continued to increase to a peak of 5367.1 kN. This was due to a large deflection of the column at this stage, and the continuous decrease of horizontal distance at the beam end weakened the influence of shock wave on the axial force, and the axial force increased to the peak value and fluctuates. At the same time, the drop hammer was still moving downward, continuing to produce a downward force on the column. In the descending stage, the axial force began to increase again, and the support reaction force rapidly offloaded and increased in reverse. This was because at this stage, the column began to rebound, the horizontal distance of the beam end increased, and gradually approached the initial length, so that the axial force increased again. At the same time, the drop hammer also began to rebound, no longer producing downward impact force on the column, so that the support reaction force was quickly unloaded. When the column bounces back to the initial state, it would still move upward due to inertia, making the reaction force of the support increase in reverse. In the post-impact stage, the axial force and support reaction force both oscillated at a certain value due to the existence of the natural vibration of the column.

3.5 Strain distribution

Fig. 15 shows the distribution of equivalent plastic strain of the steel tube and concrete. As shown in Fig. 15, the plastic strain of the steel tube was mainly concentrated in the impact zone and extending to the support on both sides, and a "drum-like" plastic concentration zone was formed in the middle of the cable-stayed zone. This was because the column height was large resulted in relatively large shear span ratio. However, the impact energy was large and its action time was short. The weak stress in the middle of the cable-stayed area developed rapidly and diffused around, forming a “Plastic Drum”. The plastic strain of steel profiles was low and mainly concentrated in the area between the middle span and the support. The maximum plastic strain of concrete mainly concentrated in the middle span, and extended to both sides of the support as a stripy-like area. The results show that the deformation modes of steel tube, concrete, and steel profiles were relatively consistent, and they bear the impact load together. Among them, the steel tube has a large strain and high energy consumption, which can protect the core concrete during impact. At the same time, the internal cross steel profiles can enhance the stiffness of the column and effectively reduce the concrete strain.

4 Parametric analyses

4.1 Mass of drop hammer

Figs. 16 and 17 show the impact force time history curve and deflection time history curve of the column under a different mass of drop hammer impact. The mass of drop hammers M1 to M4 were 579.4 kg, 1158.7 kg, 1738.1 kg, and 2317.4 kg, respectively. It can be seen from the figure that with the increase of drop hammer mass, the peak impact force of column did not increase significantly. From M1 to M4, when the drop hammer mass increased by 3 times, the peak impact force only increased by 14.5 %, this is because the contact stiffness between the drop hammer and the column is almost unchanged. By contrast, the impact force at the plateau stage increased considerably, from about 1.7 MN to 2.9 MN, an increase of 70.6 %. This is because the interaction between the drop hammer and the column enhanced with the increase of inertial force, which increased the impact force and impact time at the plateau stage. At the same time, the maximum deflection and residual deflection of the column were increased. The maximum deflection and residual deflection of M4 column are 2.8 and 3.2 times of those of M1 column, respectively. The moment when the column reaches the maximum deflection increases from 0.0075 s to 0.0130 s. This is due to the greater interaction force and longer interaction time between the heavy drop hammer and the column.

4.2 Impact momentum

Impact energy is an important factor affecting the impact process of column. However, when the impact energy is the same and the impact momentum is different, the dynamic response produced by the column is also different. Therefore, the drop weight mass and impact velocity are adjusted at the same time to ensure that the energy of each impact is the same but the momentum is different, and the impact dynamic response of the column is studied. Table 3 lists the variable parameters for the different columns.

Figs. 18 and 19 show the impact force time history curve and mid-span deflection time history curve of the column under fire in the same impact energy but different momentum. It can be seen that the impact dynamic response of the column under different momentum shows great difference. The larger the momentum is, the smaller the peak impact force is, and the larger the impact value is in the plateau stage. When the impact momentum was doubled, the peak impact force decreased by 35.2 %. This was because under the premise of the same impact energy, when the momentum increased, the impact velocity of the drop hammer would decrease, and the action time when contacting the column increased. According to the momentum theorem: $\Delta p = F \Delta t$ (Δp represents the change of momentum,

F represents the impact force, and Δt represents the change of action time), the impact force generated by the column would be reduced. At the same time, under the premise of the same impact energy, the column drop hammer with larger momentum had larger mass, larger inertia force, and stronger continuous impact on the column, making the impact value of the column plateau stage larger, increased by 27 % from about 2.2 MN to 2.8 MN. It is worth noting that the maximum deflection and residual deflection of all columns were almost the same. This was because the energy of impact was the same, and the energy of deformation converted into the column was the same, which conformed to the energy conservation law.

4.3 Fire duration

Figs. 20 and 21 show the time history curves of impact force and mid-span deflection under different fire durations. FT-1h, FT-2h, and FT-3h represent specimens with fire durations of 1 hour, 2 hours, and 3 hours, respectively. From the figure, it is evident that the fire duration greatly influences the impact resistance of the specimens. The peak impact force decreased by 85 % from 17.7 MN to 2.6 MN when the fire duration increased from 1 hour to 3 hours. The maximum mid-span deflection increased by 39 % from 18.3 mm to 25.4 mm. The impact time increased from 0.0066 seconds to 0.0112 seconds at the same time. As a result of effects of high temperature, the specimen material gradually deteriorates, and the contact stiffness between the drop hammer and the specimen is greatly reduced when the impact happens, resulting in a greater reduction in peak impact force. Additionally, the decrease in stiffness of the specimen weakens the impact resistance, so that the maximum mid-span deflection increases, and the impact time is prolonged as a result of the longer contact time between the softened specimen and the drop hammer.

4.4 Impact velocity

Previous impact tests in the room temperature had indicated that the height or velocity of the impact has great effects on the impact response of the specimens. To assess the effects of impact velocity on the impact behavior of CSRCFST columns under fire, a series of FE models were built. Figs. 22 and 23 show the time history curves of impact force and mid-span deflections. V1, V2, V3 and V4 in the figures represent the specimens with impact velocities of 5.42 m/s, 7.67 m/s, 9.39 m/s and 10.84 m/s respectively. It can be seen from the figures that the impact velocity has a great influence on the peak impact force, the impact force of plateau stage, the mid-span deflection and the impact duration of the specimen. When the impact velocity increases from 5.42 m/s to 10.84 m/s, the peak impact force increases from 4.3 MN to 8.4 MN, increasing by 95 %. The impact force of plateau stage increases slightly, but the duration of the plateau stage increases significantly. At the same time, the maximum mid-span deflection of the specimen increased from 10.7 mm to 28.6 mm, an increase of 167 %. This is because the larger the impact velocity represents greater momentum but shorter initial contact time between the drop hammer and the specimen when the impact mass kept unchanged. According to the momentum theorem: $\Delta p = F\Delta t$, when Δp increases and Δt decreases, F will be larger. At the same time, greater impact velocity is accompanied by greater impact energy, which is converted into more strain energy of the specimen, and the conversion time is longer.

5 Conclusion

In this paper, the FE numerical simulation was carried out to quantify the impact response of CSRCFST column under room temperature and fire. The model was validated and calibrated using existing tests. Using the validated FE model, the impact dynamic response of the column under fire was studied, and the parameters such as drop weight, impact momentum, fire duration, and impact velocity were analyzed. The following conclusions are drawn:

1. The numerical results of the impact test under room temperature and the fire are both in good agreement with the experimental results, and the established model is reasonable and effective.
2. The impact process of CSRCFST columns under fire can be divided into peak stage, plateau stage, descending stage, and post-impact stage. The peak stage and the plateau stage are the main impact stages. The kinetic energy is obviously transformed, consuming 32.4 % and 67.6 % of impact kinetic energy, respectively. The axial force and support reaction force response are also the largest, with peak values of 1895.6 kN and 5367.1 kN in the peak stage and plateau stage respectively.
3. Steel tube, concrete, and steel profile worked together to resist impact under fire. The steel tube has a large strain and a lot of energy consumption. The internal cross steel profile can enhance the column stiffness, which can protect the core concrete and reduce the strain.
4. The mass of drop weight is an important factor affecting the impact performance of CSRCFST columns under fire, and the impact on deflection is greater than impact force. When the mass of drop weight increases by 3 times, the maximum mid-span deflection and residual deformation increase by 2.8 and 3.2 times respectively, and the impact force at the plateau stage increase by 70.6 %, but the peak impact force only increases by 14.5 %.
5. When the impact kinetic energy is constant, the impact momentum is negatively correlated with the peak impact force of the column. When the impact momentum is doubled, the peak impact force decreases by 35.18 %. The maximum deflection and residual deflection in the column span are consistent with the impact energy.

6. The increase of fire duration will seriously deteriorate the impact performance of CSR CFSR columns, which will greatly reduce the peak impact force and increase the mid-span deflection; The change of impact velocity has an influence on the whole impact process of CSR CFST column, and is positively related to the peak impact force, platform stage impact force and mid-span deflection.
7. Overall, CSRCFST columns have good impact resistance under fire. Therefore, in the test or practical engineering design, it can be considered to add cross steel profile to CFST columns to enhance the fire resistance and impact resistance of the columns.

Acknowledgements

This research was supported by a research grant provided by the Natural Science Foundation of China (Nos. 52022024), and Guangxi Key Laboratory Project of New Energy and Building Energy Saving (Gui Ke Neng22-J-21-3 and 2021GXNSFFA196001). Any opinions, findings and conclusions expressed in this paper do not necessarily reflect the view of Natural Science Foundation of China.

References

[1] ASCE/SEI 7-10, Minimum design loads for buildings and other structures[S]. Reston, VA: American Society of Civil Engineers, 2010: 1-650.

[2] CECS 392: 2014, Code for anti-collapse design of building structures[S]. Beijing: China Planning Press, 2014: 1-117. (in Chinese)

[3] K. Qian, B. Li, Dynamic performance of RC beam-column substructures under the scenario of the loss of a corner column-Experimental results[J]. Engineering Structures, 2012, 42(Sep.): 154-167.

[4] K. Qian, B. Li, J.X. Ma, Load-carrying mechanism to resist progressive collapse of RC

buildings[J]. Journal of Structural Engineering, 2015, 141(2): 04014107.1-04014107.14.

[5] K. Qian, Z. Li, Y.H. Weng, et al, Study on continuous collapse resistance of reinforced concrete beam slab substructure[J]. Engineering Mechanics, 2019, 36(6): 239-247. (in Chinese)

[6] K. Qian, X.Y. Chen, T. Huang, Dynamic response of RC beam-slab substructures following instantaneous removal of columns[J]. Journal of Building Engineering, 2022, 45(Jan.): 103554.

[7] K. Qian, S.Y. Geng, S.L. Liang, et al, Effects of loading regimes on the structural behavior of RC beam-column sub-assemblages against disproportionate collapse[J]. Engineering Structures, 2022, 251(Part A): 113470.

[8] Y.H. Weng, K. Qian, F. Fu, et al, Numerical investigation on load redistribution capacity of flat slab substructures to resist progressive collapse[J]. Journal of Building Engineering, 2020, 29(May): 101109.

[9] FEMA. FEMA 403: World Trade Centre building performance study: data collection, preliminary observations, and recommendations[R]. Washington DC: Federal Emergency Management Agency, Federal Insurance and Mitigation Administration, 2002, Chapter 8: 1-10.

[10] NIST. NIST NCSTAR 1: Federal Building and fire safety investigation of the World Trade Center Disaster: final report on the collapse of the World Trade Center Towers [R]. Washington DC: National Institute of Standards and Technology, 2005, 155-172.

[11] Q.X. Wang, D.Z. Zhao, P. Guan, Experimental study on the strength and ductility of steel tubular columns filled with steel-reinforced concrete[J]. Engineering Structures, 2004, 26(7):907-915.

[12] A.H. Varma, J.M. Ricles, R. Sause, et al, Seismic behavior and modeling of high-strength composite concrete-filled steel tube (CFT) beam-columns[J]. Journal of Constructional Steel Research, 2002, 58(5-8): 725-758.

[13] A. Elremaily, A. Azizinamini, Behavior and strength of circular concrete-filled tube columns[J]. Journal of Constructional Steel Research, 2002, 58(12):1567-1591.
[14] R. Wang, L.H. Han, C.C. Hou, Experimental study on the behaviour of concrete filled steel tubular (CFST) members under lateral impact[C]. Structures Under Shock and Impact, 2012, 126: 241-248.
[15] L.H. Han, C.C. Hou, X.L. Zhao, et al, Behaviour of high-strength concrete filled steel tubes under transverse impact loading[J]. Journal of Constructional Steel Research, 2014, 92(Jan.):25-39.
[16] A. Al-Rifaie, S.W. Jones, Q.Y. Wang, et al, Experimental and numerical study on lateral impact response of concrete filled steel tube columns with end plate connections[J]. International Journal of Impact Engineering, 2018, 121(Nov.):20-34.
[17] X. Zhu, M. Kang, Y.F. Fei, et al, Impact behavior of concrete-filled steel tube with cruciform reinforcing steel under lateral impact load[J]. Engineering Structures, 2021, 247(15 Nov.): 113104.
[18] L.R. Li, Study on surface thermal radiation characteristics and fire thermal response behavior of concrete filled steel tubular columns[D]. Sichuan MY: Southwest University of Science and Technology, 2020, 1-75. (in Chinese)
[19] K. Li, L.X. Liu, Finite element analysis of fire resistance of concrete filled steel tubular columns under fire[J]. Industrial Safety and Environmental Protection, 2022,48 (02): 1-5. (in Chinese)
[20] X. Wang, Study on fire resistance of concrete filled steel tubular columns considering initial defects[D]. Jiangsu XZ: China University of Mining and Technology, 2020, 1-98. (in Chinese)
[21] S.H. Ji, W.D. Wang, W. Xian, Study on mechanical behavior of concrete-filled circular steel tubular columns with internal section steel under lateral impact load after fire[J]. Journal of

Building Structure, 2021, 42 (S2): 314-321. (in Chinese)

[22] M.C. Zhu, F.Q. Meng, B.J. He, Experimental study on fire resistance of steel reinforced concrete filled steel tubular columns[J]. Journal of Building Structure, 2016, 37(3): 36-43. (in Chinese)

[23] ISO 834:1975, Fire-resistance tests-Elements of building construction[S]. Switzerland GVA, International Organization for Standardization, 1975.

[24] L.H. Han, X.L. Zhao, Z. Tao, Tests and mechanics model for concrete-filled SHS stub columns, columns and beam-columns[J]. Steel and Composite Structures, 2001, 1(1): 51-74.

[25] R. Wang, L.H. Han, C.C. Hou, Behavior of concrete filled steel tubular (CFST) members under lateral impact: experiment and FEA model[J]. Journal of Constructional Steel Research, 2013, 80(1): 188-201.

[26] C.C. Hou, L.H. Han, Life-cycle performance of deteriorated concrete-filled steel tubular (CFST) structures subject to lateral impact[J]. Thin-Walled Structures, 2018, 132(Nov.): 362-374.

[27] L.H. Han, Concrete filled steel tubular structures-theory and practice(third edition)[M]. Beijing: Science Press, 2016: 1-997. (in Chinese).

[28] GB 51249-2017, Technical code for fire protection of building steel structures[S]. Beijing: China Planning Press, 2017: 1-120. (in Chinese）

[29] T.T. Lie, Fire resistance of circular steel columns filled with Bar-Reinforced concrete[J]. Journal of Structural Engineering, 1994, 120(5): 1489-1509.

[30] Z. Tao, X.Q. Wang, B. Uy, Stress-strain curves of structural and reinforcing steels after exposure to elevated temperatures[J]. Journal of Materials in Civil Engineering, 2013, 25(9):1306-1316.

TABLES AND FIGURES

List of Tables:

List of Figures:

Figure. 16. Time history curve of impact force

Figure. 17. Time history curve of mid-span deflection

Figure. 18. Time history curve of impact force

Figure. 19. Time history curve of mid-span deflection

Table 1- Typical column variable parameters of room temperature impact field

Specimen label	*H* (m)	*V* (m/s)	*n*
S8MFF0	3.0	7.67	0.0
S8HFF1	4.5	9.39	0.1
S8HFF2	4.5	9.39	0.2

Table 2- Steel properties

t (mm)	f_y (MPa)	f_u (MPa)	E_s (MPa)	δ (%)
6	427.0	625.3	2.10×10^5	22.2
8	400.6	564.0	$2.06 \times 10_5$	21.3
9	358.2	529.4	2.03×10^5	23.0

Table 3-Specimen properties

Specimen label	Drop hammer quality (kg)	Impact velocity (m/s)	Impact energy (kJ)	Impact momentum (kg·m/s)
E-P1	869.4	10.84	51.1	9424.3
E-P2	1158.7	9.39	51.1	10880.2
E-P3	1736.6	7.67	51.1	13319.8
E-P4	3477.8	5.42	51.1	18849.7

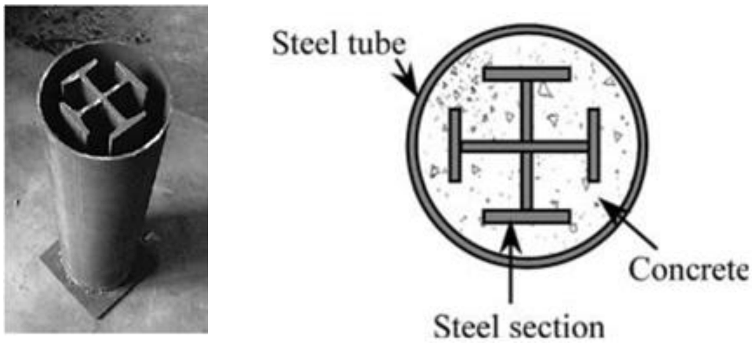

Figure. 1. New CSRCFST structure from [11]

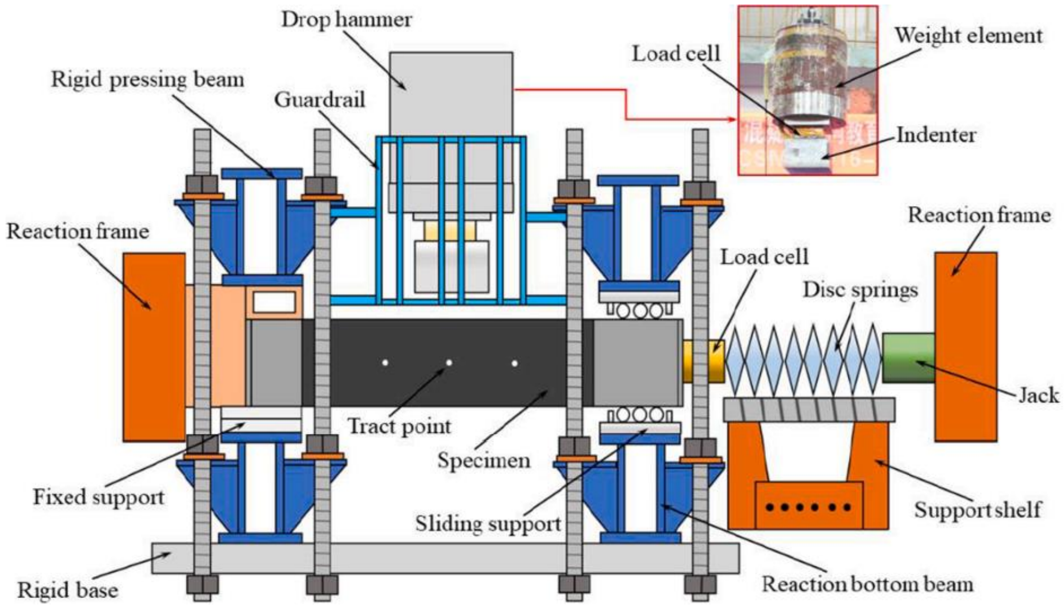

Figure. 2. Room temperature impact test device in [17]

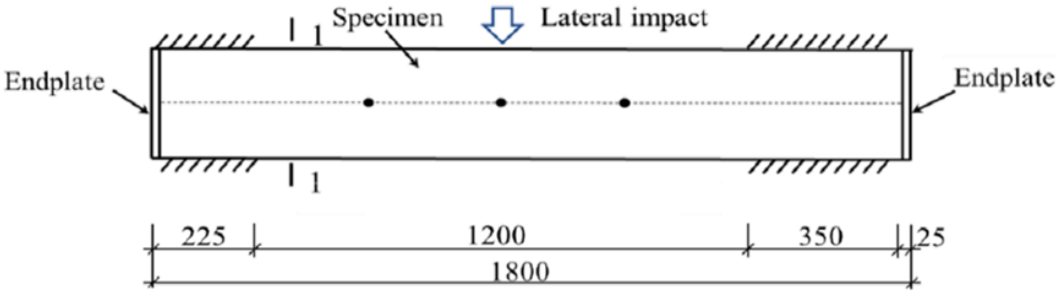

(a)

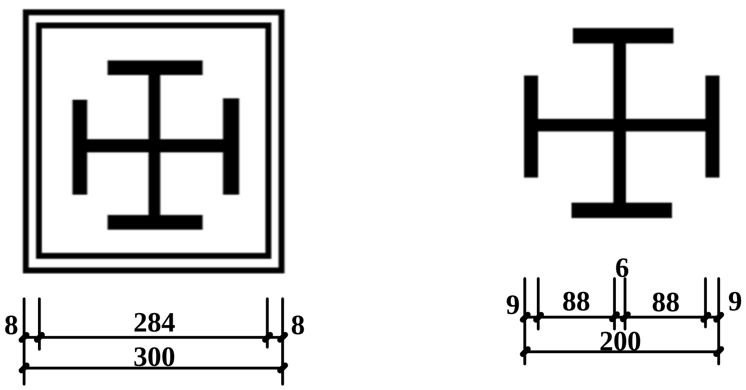

(b)

Figure. 3. CSRCFST column details and section dimension [17]: (a) column details; (b) column section dimension

Figure. 4. Fire test device in [22]

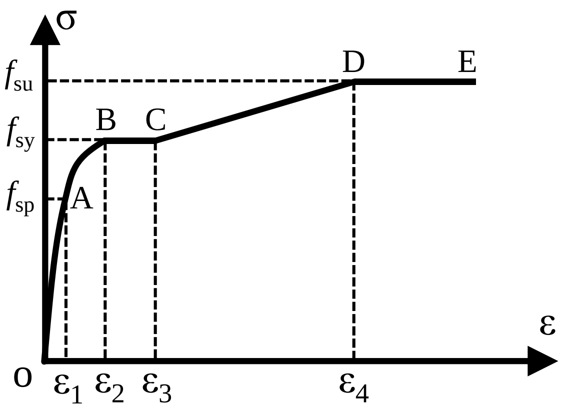

Figure. 5. Stress-strain curve of the steel [24]

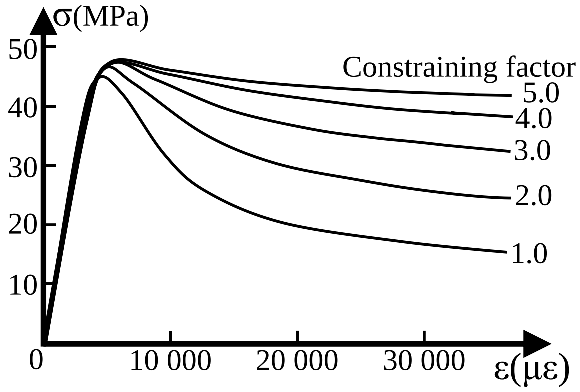

Figure. 6. Stress-strain curves of concrete in different constraining factors [24]

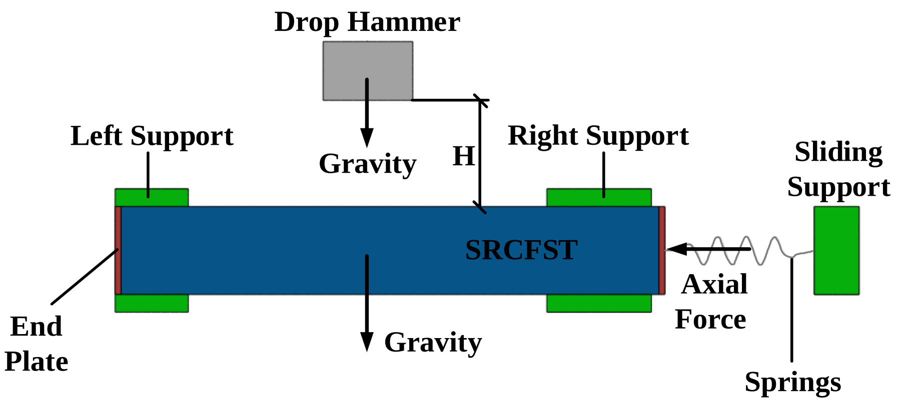

Figure. 7. Model for impact test under room temperature

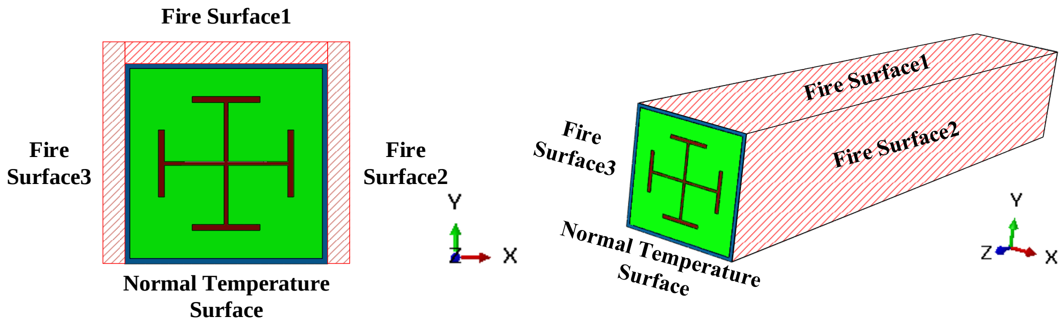

Figure. 8. Heat transferring analysis model

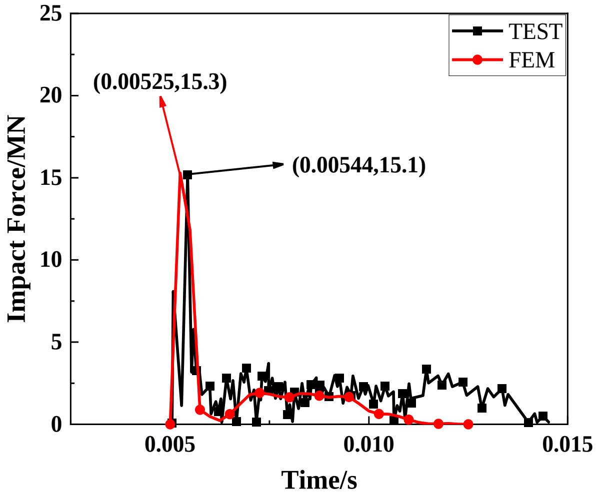
Impact Force/MN
Time/s
TEST
FEM
(0.00525,15.3)
(0.00544,15.1)
0
5
10
15
20
25
0.005
0.010
0.015

(a)

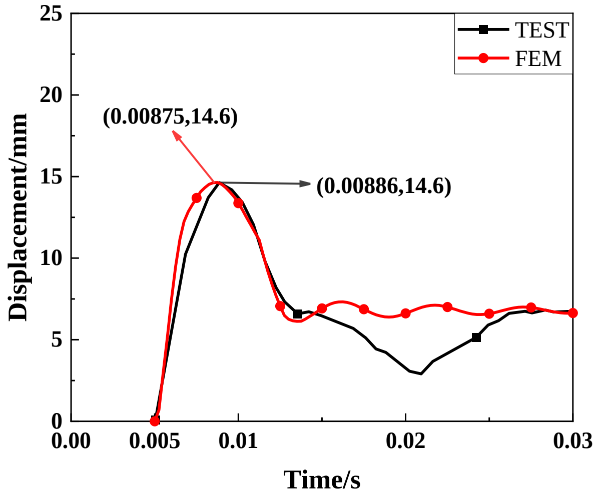
Displacement/mm
Time/s
TEST
FEM
(0.00875,14.6)
(0.00886,14.6)
0
5
10
15
20
25
0.00
0.005
0.01
0.02
0.03

(b)

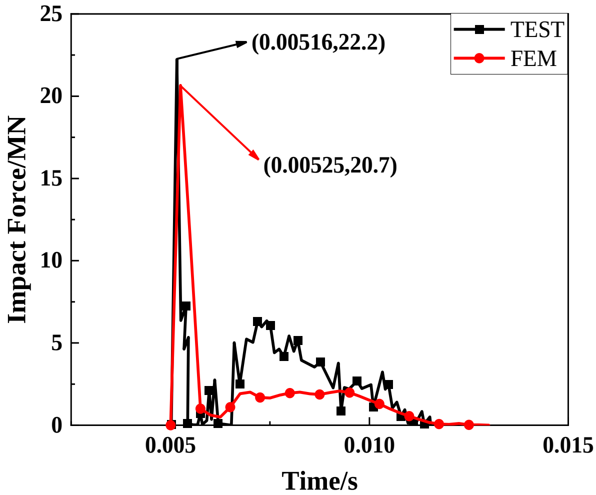
Impact Force/MN
Time/s
TEST
FEM
(0.00516,22.2)
(0.00525,20.7)
0
5
10
15
20
25
0.005
0.010
0.015

(c)

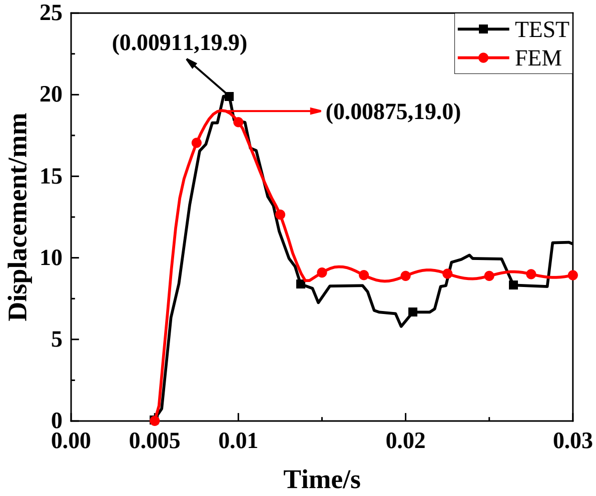

(d)

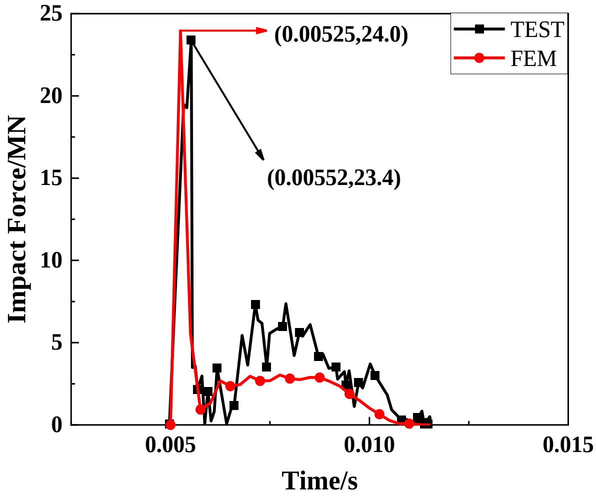

(e)

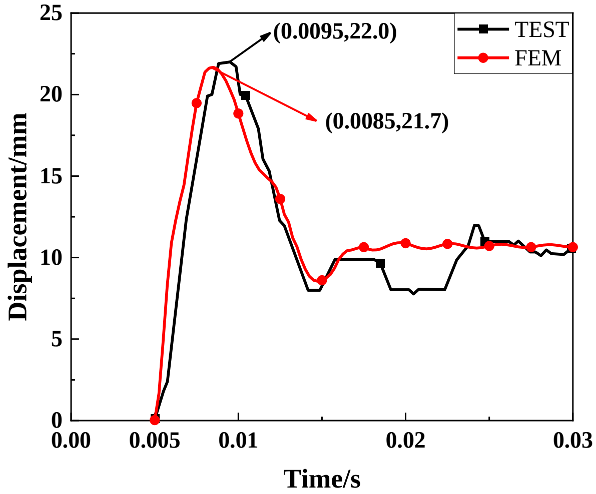

(f)

Figure. 9. Comparison of time history curves of impact force and mid-span deflection of impact columns: (a) S8MFF0; (b) S8MFF0; (c) S8HFF1; (d) S8HFF1; (e) S8HFF2; and (f) S8HFF2

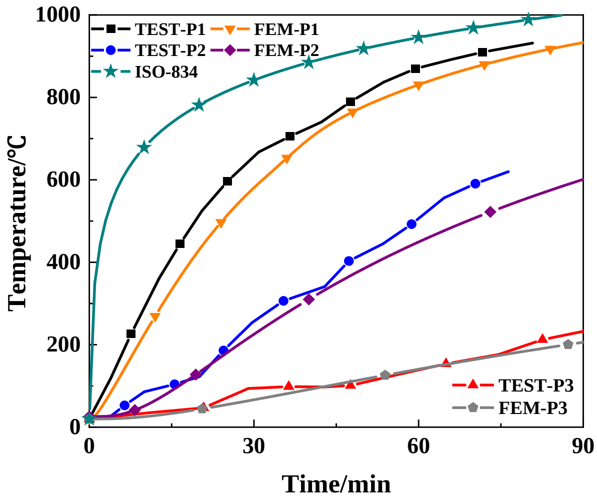

(a)

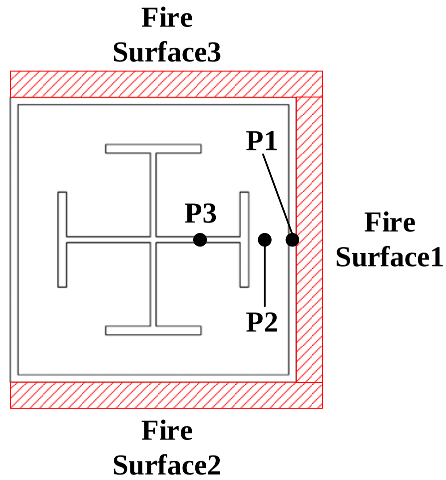

(b)

Figure. 10. Time temperature curves at different measuring points of fire components: (a) temperature rise time history curve; (b) temperature measuring point location

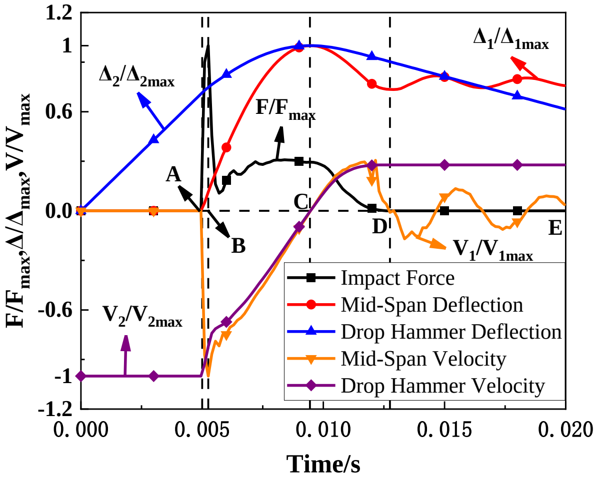

Figure. 11. Dimensionless time history curve

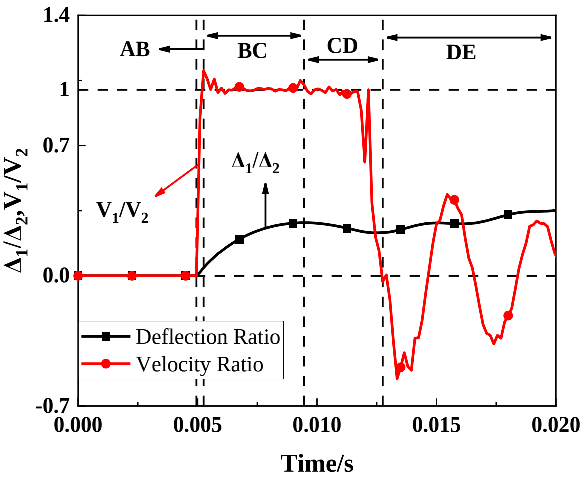

Figure. 12. Time history curve of displacement velocity ratio

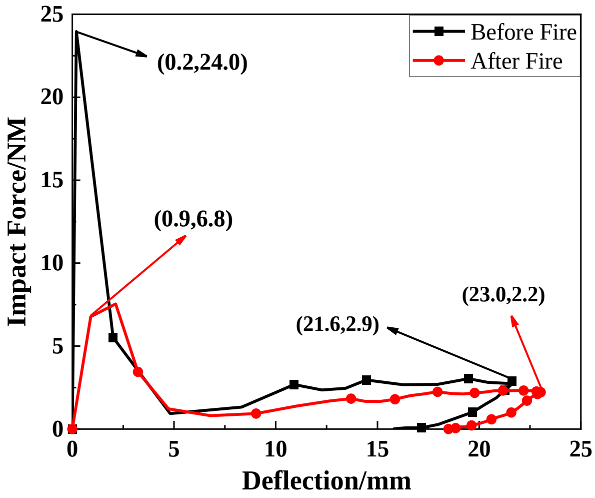

Figure. 13. Time history curve of impact force - mid-span deflection

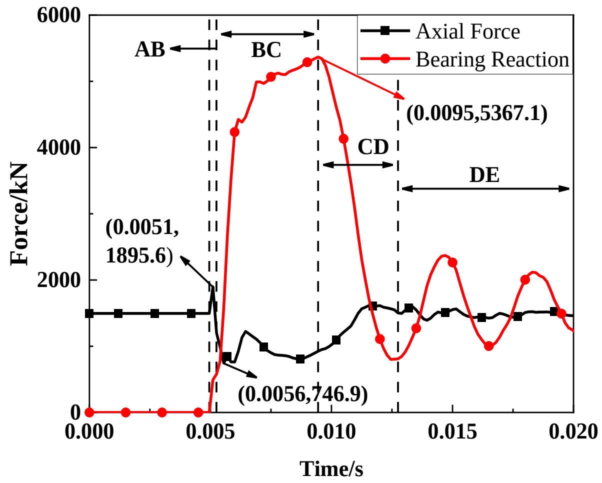

Figure. 14. Time history curve of axial force and support reaction force

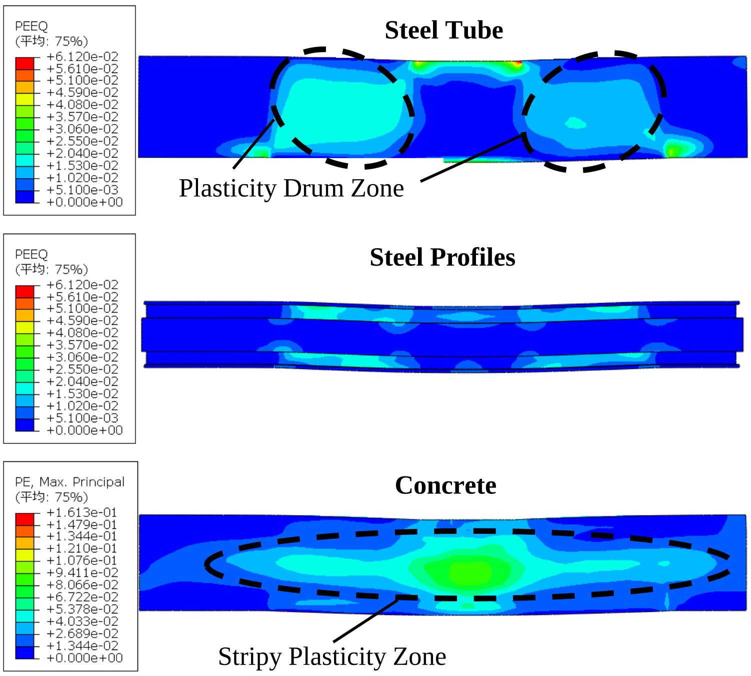

Figure. 15. Strain nephogram

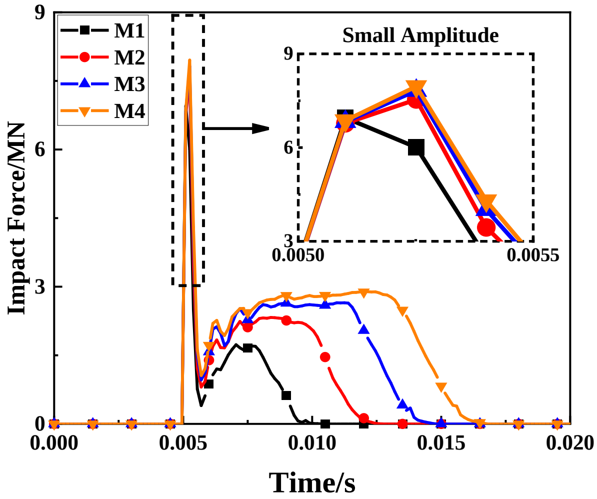

Figure. 16. Time history curve of impact force

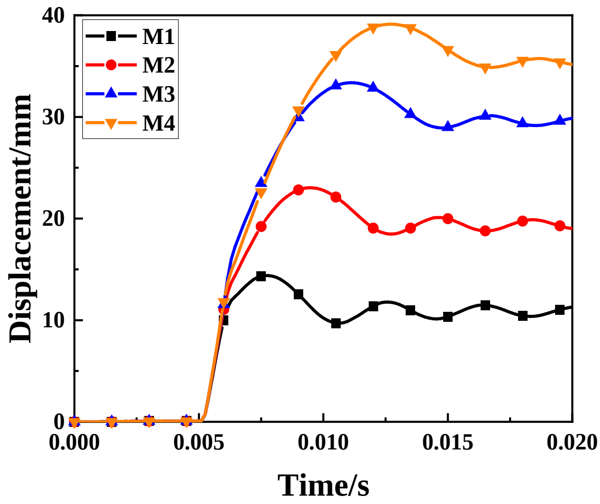

Figure. 17. Time history curve of mid-span deflection

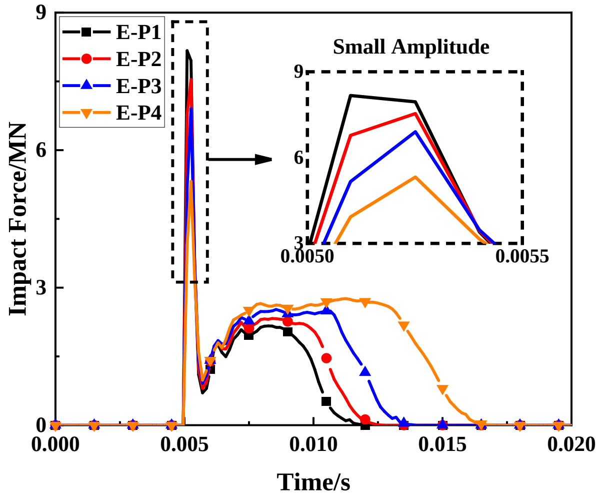

Figure. 18. Time history curve of impact force

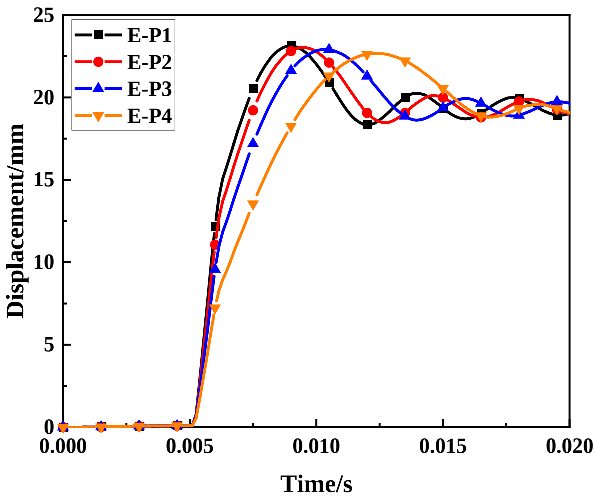

Figure. 19. Time history curve of mid-span deflection

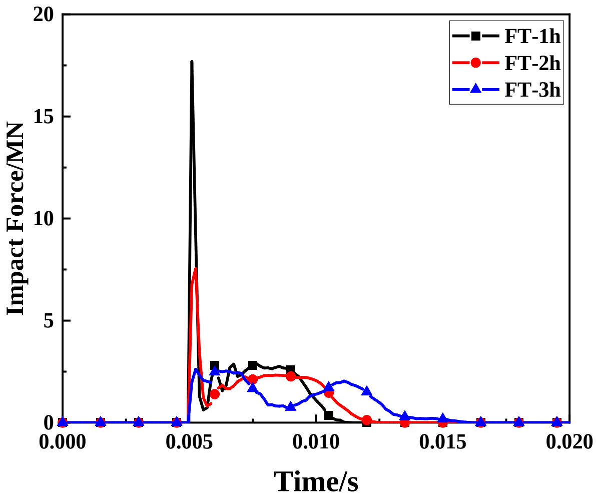

Figure. 20. Time history curve of impact force

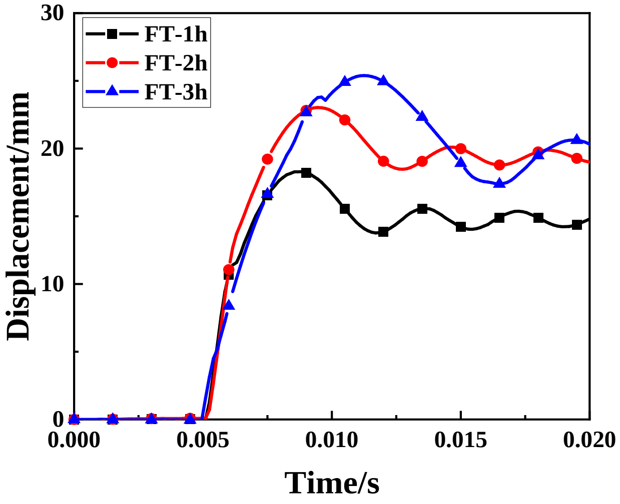

Figure. 21. Time history curve of mid-span deflection

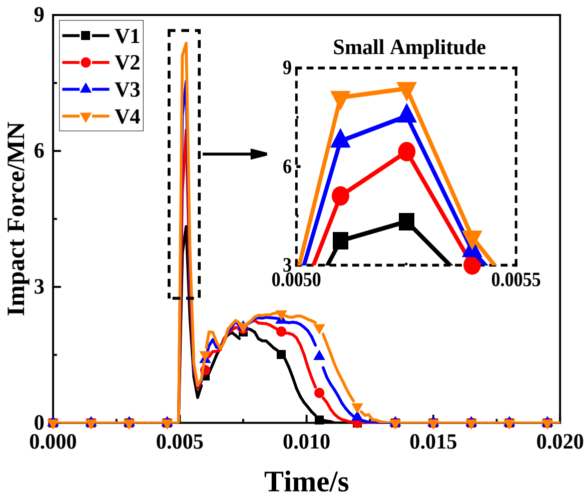

Figure. 22. Time history curve of impact force

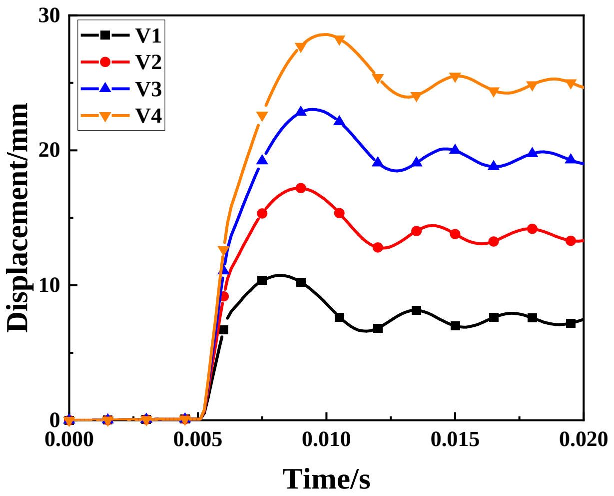

Figure. 23. Time history curve of mid-span deflection